Electron capture by a metastable ion in the collision $Ar^{8+}(2p^5 3s)^3P_{0,2}+H_2$ at low velocity

S. Bliman
Universite de Marne la Vallee, 5 Boulevard Descartes, Champs sur Marne, 77454 Marne la Vallee Cedex 2, France

M. Cornille
DARC Observatoire de Paris, CNRS UMR 8629, 92195 Meudon Cedex, France

B. A. Huber
Département de Recherche Fondamentale sur la Matière Condensée, S12A, CEA-Grenoble, 17 rue des Martyrs, 38054 Grenoble Cedex 9, France

J. Nordgren and J. E. Rubensson
Department of Physics, Uppsala University, Box 530, S7521 Uppsala, Sweden
(Received 20 January 1999; revised manuscript received 30 June 2000; published 12 February 2001)

Single-electron (SC) and double-electron capture (DC) in collisions of metastable Ar^{8+} ions with H_2 have been studied by using X-VUV and Auger spectroscopy at 10 keV per charge. SC by the long-lived metastable ion $Ar^{8+}(2p^5 3s)^3P_{0,2}$ mostly populates inner-shell excited Na-like $Ar^{7+}**[(2p^5 3s)^3P, nl]^{2,4}L_j$ levels with $n=5$, a small fraction going to $n=4$. With the use of radiative and Auger decay rates, the observed X-VUV and Auger spectra are analyzed and compared with the spectra obtained by other authors. It is shown that the stabilization of these core-excited states is both radiative and autoionizing. DC by the metastable projectile reveals the formation of triply excited $Ar^{6+}***$ ions. They stabilize along two Auger decay steps: the first one gives a low-energy electron, associated with the decay to the intermediate continua $Ar^{7+}(2p^5 3l3l')$, while the second step—originating from these $Ar^{7+}(2p^5 3l3l')$ levels—gives a higher-energy electron, characteristic of the decay to the only available continuum $Ar^{8+}(2p^6)^1S_0$.

DOI: 10.1103/PhysRevA.63.032710 PACS number(s): 34.70.+e, 32.90.+a

I. INTRODUCTION

Most charge-exchange collisions, studied at low energies ($E<25$ keV/amu), have been performed with projectiles (highly charged ions) in their ground states, neglecting the presence of metastable ions in the primary beam.

However, many studies have shown that the single-electron capture (SC) mechanisms for a given ion species in its ground state and in an excited metastable state lead to the population of the same n levels (principal quantum number). The corresponding cross sections are the same. However, the stabilization mechanisms are different: for the ground-state projectile only radiative decay occurs; for the metastable ion, both radiative and Auger decays are possible. In the latter case extended sets of atomic data are needed in order to ease assignments and identify the observed transitions. In general, a theoretical cross-section determination has not been done and we are left with experimental scaling rules for predicting which levels are mostly populated: (n,l) (principal and orbital quantum numbers).

When dealing with double-electron capture (DC), the situation is more complex. Collisions with ground-state projectiles end in doubly excited states while with metastable ions they end in triply excited states. As was shown in Ref. [1] for the system $Ar^{8+}(2p^5 3s)^3P^0+He$, the levels which are dominantly populated were identified to be above the second ionization limit of Ar^{6+}.

The difficulties that frequently arise in studying systems involving metastable ions are twofold.

(a) Experimentally, the ion beams, normally produced by electron cyclotron resonance (ECR) ion sources contain low metastable fractions and thus long acquisition times are required, even with high sensitivity devices. To circumvent this experimental difficulty, beams of ions X^{9+} with highly enriched metastable fractions can be prepared by SC, starting out with beams of initial charge $(q+1)$. For example, an enriched metastable beam of $O^{6+}(1s2s)^3S_1$ can be prepared by the following process:

$$O^{7+}(1s)^2S_{1/2}+X \ \ (\text{any target}) \rightarrow O^{6+}(1s\,nl)^{1,3}L_J+X^+. \tag{1}$$

This reaction is followed by the radiative cascade decay to both the ground state $O^{6+}(1s^2)^1S_0$ [some fraction ends in $O^{6+}(1s2s)^1S_0$, the lifetime of which is shorter than that of $O^{6+}(1s2s)^3S_1$ and which decays via two-photon emission] and the metastable state $O^{6+}(1s2s)^3S_1$, where statistical sharing among singlet and triplet states enhances the metastable fraction. This procedure was used to facilitate the translational energy gain spectroscopy measurement [2]. Among the experimental approaches, Auger spectroscopy is frequently chosen. In the case of SC ending in core-excited ions, this method allows easy identification of the transitions. However, ambiguities may arise in the case of DC, lines are observed and improperly attributed, i.e., lines are attributed to SC which in fact result from one step in a two-step cascade from triply excited levels [1].

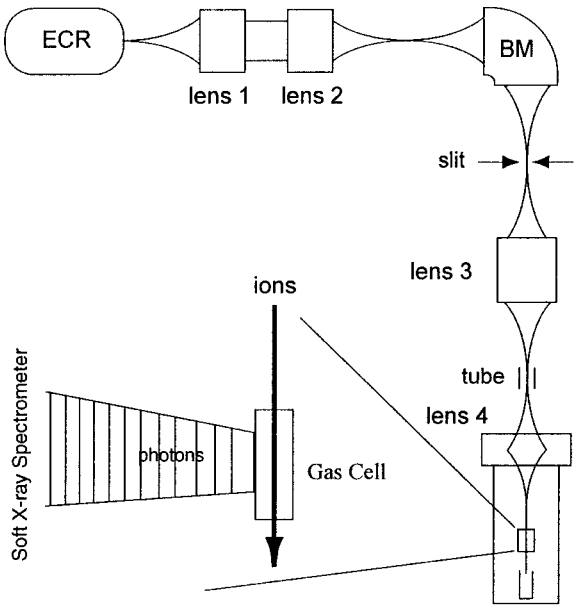

FIG. 1. Schematic of the experimental device: the ion beam extracted from the ECR ion source is mass and charge analyzed using a bending magnet (BM) and then passed into the gas cell. The spectrometer is attracted to the collision cell to detect the emitted photons resulting from the excited ions formed in the capture process.

(b) Theoretically, the calculation of atomic data (energy levels, radiative and Auger decay rates) for doubly and triply excited states is not straightforward even with the most sophisticated codes (in Ref. [3] three different theoretical approaches and codes are compared). Moreover, for triply excited ions there is no fully reliable theoretical description.

For the collision system

$$Ar^{8+}(2p^5 3s)^3P_{0,2} + H_2 \tag{2}$$

we present the experimental arrangements and methods in Sec. II. Section III outlines the atomic data calculations; they allow better line identifications, both in the X-VUV and the Auger spectra. Section IV focuses on the collision features.

II. EXPERIMENTAL ARRANGEMENTS AND METHODS

The experimental device (see Fig. 1) basically uses an ECR ion source that delivers multiply charged ion beams. Once accelerated, with use of a bending magnet (BM), they are mass and charge analyzed to sort out the specific ions needed. Then the selected beam is passed in a differentially pumped collision cell where SC and DC take place. The gas pressure, monitored using a Baratron, is kept at a value such that the single collision condition is satisfied ($p \approx 1.5-2 \times 10^{-5}$ mbar of H_2).

The collision system $Ar^{8+}+H_2$ is studied using and comparing two different experimental methods. On the one hand, X-VUV spectroscopy is applied at a collision energy of 80 keV. The grazing incidence spectrometer is set at 90° to the beam direction, looking directly into the collision chamber and thus yielding information on the decay of the populated

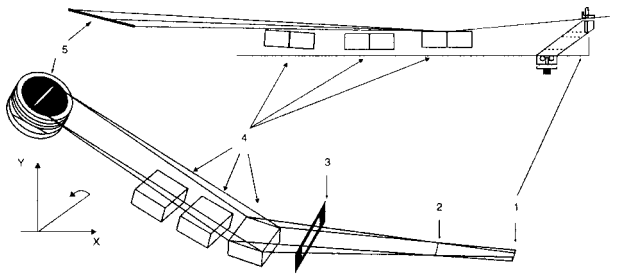

FIG. 2. Schematic of the XUV grazing incidence spectrometer: 1, interaction region; 2, entrance slit; 3, grating selector; 4, gratings; 5, detector based on multichannel plates. Upper part, lateral view; lower part, vertical view.

excited states. On the other hand, the ions resulting from the collision processes are studied with the aid of the Auger spectroscopy technique at the same collision energy. This second method gives access to the states formed in the collision. In the following, we give a brief description of both experimental arrangements.

A. X-VUV spectroscopy

An argon-ion beam delivered by the ECR ion source at the AIM facility (of CEA-Grenoble) is charge and mass analyzed in order to obtain a pure Ar^{8+} beam. The typical ion current is 5 μA at 80 keV (ion velocity $v \approx 0.28$ a.u.). The ion beam passes in the differentially pumped collision chamber; the base pressure in the surrounding space is kept as low as 1.5×10^{-8} Torr. It has been shown that the metastable fraction content of the primary ion beam is of the order of 5–6 % [2,4]. A schematic view of the grazing incidence spectrometer is shown in Fig. 2. The observation wavelength window is set below 55 Å and the spectrum shown in Fig. 3 is unambiguously interpreted as resulting from electron capture by $Ar^{8+}*(2p^5 3s)^3P_{0,2}$ ions. The compact core one outer excited electron Ar^{7+} emission spectrum limit is 81.3 Å. For wavelength calibration, a spectrum was taken of the X-VUV radiative decay of the products of the SC reaction

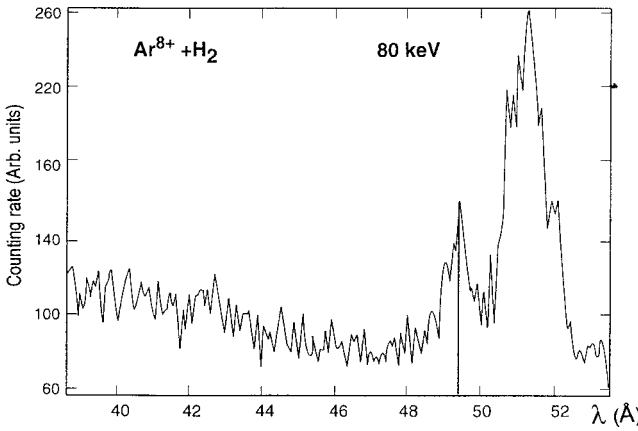

FIG. 3. Normalized intensity (in counts) of the x-ray spectrum emitted by the products of the SC collision. $Ar^{8+}(2p^5 3s)^3P_{0,2} + H_2 \rightarrow Ar^{7+}(2p^5 3snl)^{2,4}L_J + H_2^+$ versus wavelength (recorded in the window 40–54 Å).

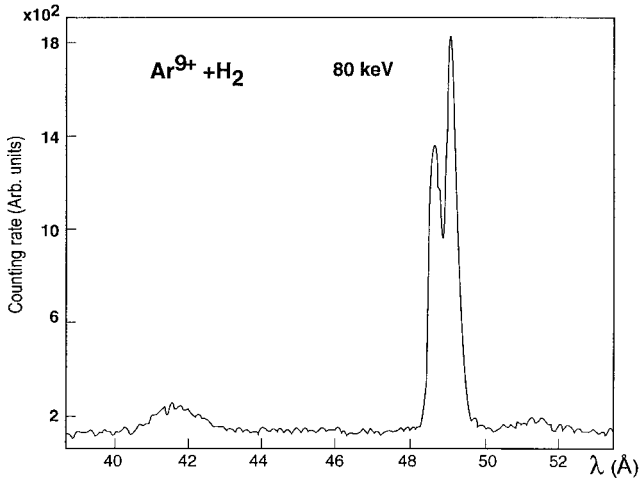

FIG. 4. Normalized intensity (in counts) of the x-ray spectrum emitted by the products of the SC collision. $Ar^{9+}(2p^5)+H_2 \rightarrow Ar^{8+}(2p^5nl)^{1,3}L_J+H_2^+$ versus wavelength (recorded in the window 40–54 Å). The weaker peak is identified as the transition $Ar^{8+}(2p^53s)^1P_1 \rightarrow Ar^{8+}(2p^6)^1S_0$, the higher intensity one as $Ar^{8+}(2p^53s)^3P_1 \rightarrow Ar^{8+}(2p^6)^1S_0$.

$$Ar^{9+}+H_2 \rightarrow Ar^{8+}(nl)^{1,3}L_J+H_2^+ \tag{3}$$

and ending in the emission of the resonant Ne-like rays,

$$Ar^{8+}(2p^53s)^{1,3}P_1 \rightarrow Ar^{8+}(2p^6)^1S_0+h\nu. \tag{4}$$

A typical spectrum for Ar^{9+}/H_2, obtained in the same wavelength interval as in Fig. 3, is shown in Fig. 4.

B. Auger spectroscopy

Under similar experimental conditions, Mack [5] at KVI (Groningen, The Netherlands) and Boudjema [6] at the AIM (Grenoble, France) recorded the same Auger-electron spectra, where gross peak identifications were only suggested. A typical Auger-electron spectrum is presented in Fig. 5. Clearly two energy regions appear in this spectrum: one below 65 eV and the other one above 102 eV and extending up

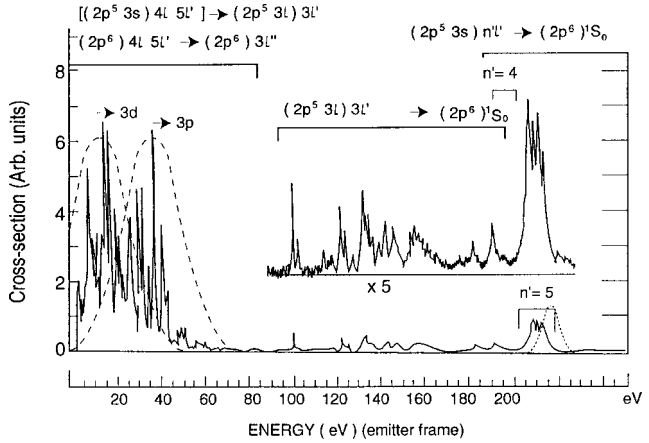

FIG. 5. Auger spectrum (arbitrary units) corresponding to the stabilization of the DC products of $Ar^{8+}(2p^53s)^3P_{0,2}+H_2 \rightarrow Ar^{6+}(2p^53snln'l')^{1,3,5}L_J+H'+H'$ versus energy (in eV). Lines attributed to the SC by the metastable ion and to the DC by the ground-state projectile are also present (see text).

to approximately 250 eV. From previous results obtained for $Ar^{8+}+He$ [1], we understand that most of the high-energy part of the spectrum is to be attributed to charge transfer(s) to the metastable projectile. Under these conditions, the scaling laws available for the prediction of the most populated levels, in SC and DC [7–11] are used to give some guidelines for the analysis.

C. Scaling predictions

Using the scaling laws established for SC and multiple captures [7–11], we have to pay special attention to the fact that we deal here with a molecular H_2 target [12] which has a different behavior than the atomic He target [2]. We have to consider SC (SC and dissociation) and DC which, respectively, will end dominantly in the population of $n=5$ and 4, $l=1$ for SC, and ($n=4$,$l=1$) and ($n'=5$,$l'=1$ and 2) for DC.

In SC the populated excited states are shared between doublets and quartets states of Ar^{7+}. In DC, the sharing can be among singlet, triplet, and quintet states of Ar^{6+}. In the following we describe the calculation procedure and present some atomic data needed for the identification of the observed transitions.

III. CALCULATION OF ATOMIC PARAMETERS

We need further data for the analysis of SC and DC as well as the line identifications. SC ends in the formation of core-excited Na-like ions; from previous observations [2] and since the collision process is core conserving we have taken into account $2p^53snl$ configurations. As understood from Ref. [1], the atomic features of $Ar^{7+}(2p^53l3l')$ are also needed and have been determined.

DC ends in core-excited Mg-like ions and there again, it is relevant to retain core conservation ending in $2p^53snln'l'$. For completeness and coherence, we have calculated the energies of the ground states of Ar^{6+},Ar^{7+} and the ionization potentials of these ions. These values are necessary for the determination of the Auger-electron energies resulting from the decays following SC and DC.

To calculate the energy levels E, wavelengths λ, radiative probabilities A_r^{ij} and the sum of all the possible radiative probabilities ΣA_r^{ij}, we used the SUPERSTRUCTURE code developed by Eissner and Nussbaumer [13]. For highly ionized elements, autoionization processes are weak enough to be treated by perturbation theory. The autoionization probability A_a^{si} is given by

$$A_a^{si}=2\pi|\langle\Psi_F^i(E_s)|H-E_s|\Psi_s\rangle|^2/(h/2\pi)^2, \tag{5}$$

where

$$E_s=\langle\Psi_s|H|\Psi_s\rangle. \tag{6}$$

Ψ_S and Ψ_F^i are the initial bound state and final free state, respectively. The autoionization probabilities are obtained using the AUTOLSJ code developed by Dubau [14]. The total fluorescence yield ω_T and the branching ratio B_r are obtained by the same code with

TABLE I. Energy levels of the core-excited Na-like argon ion relative to the ground state. Column 1: level; column 2: energy (eV) relative to the ground level; column 3: sum of Auger rates; column 4: sum of radiative transition rates; column 5: total fluorescence yield; column 6: Auger branching ratio; column 7: energy of the Auger electron for the decay to the only available continuum $Ar^{8+}(2p^6)^1S_0$. The levels with high fluorescence yields are underlined.

	Level (eV) per GS	ΣA_a (s^{-1})	ΣA_r (s^{-1})	ω^T	B_r	E_A (eV)
$1s^22s^22p^53s5s\ ^4P_{5/2}$	353.8493	2.388(01)	0	0	1	210.8493
$1s^22s^22p^53s5s\ ^4P_{3/2}$	354.2601	1.400(11)	1.764(10)	1.119(−01)	8.810(−01)	211.2601
$1s^22s^22p^53s5s\ ^2P_{1/2}$	354.8473	1.131(10)	6.212(10)	8.459(−01)	1.541(−01)	211.8473
$1s^22s^22p^53s5s\ ^2P_{3/2}$	355.0280	8.020(11)	3.360(10)	4.020(−02)	9.597(−01)	212.0280
$1s^22s^22p^53s5s\ ^4P_{1/2}$	356.0128	6.930(10)	1.854(10)	2.111(−01)	7.889(−01)	213.1288
$1s^22s^22p^53s5s\ ^2P_{3/2}$	356.9803	1.869(11)	1.342(11)	4.790(−01)	5.210(−01)	213.9803
$1s^22s^22p^53s5p\ ^4S_{3/2}$	356.8946	3.602(05)	9.688(08)	9.996(−01)	0	213.8946
$1s^22s^22p^53s5p\ ^4D_{7/2}$	357.0707	3.288(00)	1.713(08)	1	0	214.0707
$1s^22s^22p^53s5p\ ^4D_{5/2}$	357.1547	2.876(08)	7.665(08)	7.272(−01)	2.728(−01)	214.1547
$1s^22s^22p^53s5p\ ^4D_{3/2}$	357.3595	3.673(08)	4.491(09)	9.244(−01)	7.560(−02)	214.3595
$1s^22s^22p^53s5p\ ^4P_{5/2}$	357.3853	1.482(09)	9.959(08)	4.019(−01)	5.981(−01)	214.3853
$1s^22s^22p^53s5p\ ^2P_{1/2}$	357.6480	2.994(12)	1.571(10)	5.220(−03)	9.947(−01)	214.6480
$1s^22s^22p^53s5p\ ^4P_{1/2}$	357.9562	1.846(12)	5.397(10)	2.841(−02)	9.715(−01)	214.9562
$1s^22s^22p^53s5p\ ^2D_{3/2}$	357.9969	2.216(09)	4.560(10)	9.537(−01)	4.630(−02)	214.9969
$1s^22s^22p^53s5p\ ^2D_{5/2}$	358.0351	1.556(08)	4.378(10)	9.965(−01)	3.500(−02)	215.0351
$1s^22s^22p^53s5p\ ^2P_{3/2}$	358.0733	1.203(09)	3.625(10)	9.679(−01)	3.210(−02)	215.0733
$1s^22s^22p^53s5p\ ^2S_{1/2}$	358.5054	7.117(12)	2.973(10)	4.161(−03)	9.958(−01)	215.5054
$1s^22s^22p^53s5p\ ^4P_{3/2}$	359.3213	1.026(09)	4.251(09)	8.057(−01)	1.943(−02)	216.3213
$1s^22s^22p^53s5p\ ^4D_{1/2}$	359.3884	3.622(12)	2.296(10)	6.293(−03)	9.937(−01)	216.3884
$1s^22s^22p^53s5p\ ^2P_{3/2}$	360.1618	1.364(09)	1.299(11)	9.896(−01)	1.100(−04)	217.1618
$1s^22s^22p^53s5p\ ^2D_{5/2}$	360.1797	4.432(09)	1.266(11)	9.662(−01)	3.380(−04)	217.1797
$1s^22s^22p^53s5p\ ^2P_{1/2}$	360.3256	2.499(09)	1.260(11)	9.806(−01)	1.940(−04)	217.3256
$1s^22s^22p^53s5p\ ^2D_{3/2}$	360.3561	1.327(08)	1.228(11)	9.989(−01)	0	217.3561
$1s^22s^22p^53s5p\ ^2S_{1/2}$	360.8536	1.158(13)	1.077(11)	9.216(−03)	9.908(−01)	217.8536
$1s^22s^22p^53s5d\ ^4P_{1/2}$	361.0449	6.199(08)	1.160(09)	6.518(−01)	3.482(−01)	218.0449
$1s^22s^22p^53s5d\ ^4P_{1/2}$	361.1285	1.771(09)	2.528(09)	5.880(−01)	4.120(−01)	218.1285
$1s^22s^22p^53s5d\ ^4F_{9/2}$	361.1721	6.349(−01)	4.626(08)	1	0	218.1721
$1s^22s^22p^53s5d\ ^4P_{5/2}$	361.2519	4.832(08)	9.916(08)	6.728(−01)	3.272(−01)	218.2519
$1s^22s^22p^53s5d\ ^4F_{7/2}$	361.2805	3.721(10)	9.874(08)	2.585(−02)	9.741(−01)	218.2805
$1s^22s^22p^53s5d\ ^4F_{5/2}$	361.4304	4.566(10)	2.188(09)	4.582(−02)	9.541(−01)	218.4304
$1s^22s^22p^53s5d\ ^2F_{7/2}$	361.4412	1.94(11)	4.560(08)	2.282(−03)	9.977(−01)	218.4412
$1s^22s^22p^53s5d\ ^2D_{3/2}$	361.5945	4.204(10)	5.128(10)	5.495(−01)	4.505(−01)	218.5945
$1s^22s^22p^53s5d\ ^2P_{1/2}$	362.0901	2.115(11)	2.252(11)	5.157(−01)	4.843(−01)	219.0901
$1s^22s^22p^53s5d\ ^4D_{3/2}$	362.0901	6.800(07)	4.985(10)	9.986(−01)	0	219.0901
$1s^22s^22p^53s5d\ ^4D_{1/2}$	362.0927	9.558(09)	5.523(10)	8.525(−01)	1.475(−01)	219.0927
$1s^22s^22p^53s5d\ ^2D_{5/2}$	362.0947	2.539(10)	3.694(10)	5.927(−01)	4.073(−01)	219.0947
$1s^22s^22p^53s5d\ ^4D_{7/2}$	362.0972	5.993(10)	4.563(10)	4.322(−01)	5.678(−01)	219.0972
$1s^22s^22p^53s5d\ ^2F_{5/2}$	362.1502	2.501(10)	4.809(10)	3.613(−01)	6.87(−01)	219.1502
$1s^22s^22p^53s5d\ ^2P_{3/2}$	362.4818	1.790(11)	1.994(11)	5.269(−01)	4.731(−01)	219.4818
$1s^22s^22p^53s5f\ ^4D_{1/2}$	362.9968	2.380(05)	4.828(07)	9.950(−01)	0	219.9968
$1s^22s^22p^53s5f\ ^4D_{3/2}$	363.0224	4.223(09)	1.990(08)	4.500(−02)	9.550(−01)	220.0224
$1s^22s^22p^53s5f\ ^4F_{11/2}$	363.0420	0	4.314(07)	1	0	
$1s^22s^22p^53s5f\ ^4D_{5/2}$	363.0627	2.169(09)	2.702(08)	9.350(−02)	9.065(−01)	220.0627
$1s^22s^22p^53s5f\ ^4G_{9/2}$	363.0972	1.366(09)	2.854(08)	1.728(−01)	8.272(−01)	200.0972
$1s^22s^22p^53s5f\ ^4F_{7/2}$	363.1023	3.826(07)	9.676(07)	7.166(−01)	2.834(−01)	220.1023
$1s^22s^22p^53s5f\ ^4F_{9/2}$	363.2588	7.500(10)	2.006(09)	2.605(−02)	9.739(−01)	220.2588
$1s^22s^22p^53s5f\ ^4F_{3/2}$	363.2601	4.438(11)	1.953(09)	4.382(−03)	0	220.2601
$1s^22s^22p^53s5f\ ^4F_{7/2}$	363.2824	1.354(10)	3.688(09)	2.140(−01)	7.860(−01)	220.2824
$1s^22s^22p^53s5f\ ^4F_{5/2}$	363.2829	1.825(11)	3.043(08)	1.617(−02)	9.838(−01)	220.2829
$1s^22s^22p^53s5G\ ^4H_{13/2}$	363.5105	0	3.872(05)	1	0	220.5105
$1s^22s^22p^53s5G\ ^2H_{11/2}$	363.5625	3.347(09)	1.629(07)	4.843(−03)	1	220.5625

TABLE II. Energy levels of $Ar^{7+}(2p^5 3l3l')$ relative to the ground state. Column 1: configurations; column 2: energy from ground state (eV); column 3: Auger-electron energy for decay to the only available continuum $Ar^{8+}(2p^6)^1S_0$.

Configurations		Energy (eV) per GS	Energy (eV) per Auger	Configurations		Energy (eV) per GS	Energy (eV) per Auger
$2p^5 3s^2$	$^2P_{3/2}$	247.9700	105.1756		$^2D_{3/2}$	310.1021	167.3076
	$^2P_{1/2}$	250.0556	107.2612		$^2D_{5/2}$	310.2478	
$2p^5 3s3p$	$^2D_{3/2}$	263.3755	120.5018		$^2S_{1/2}$	311.2951	168.5006
	$^2P_{1/2}$	264.7091	121.9146		$^2D_{3/2}$	311.5009	168.7064
	$^2D_{5/2}$	265.0940	122.2999		$^2P_{3/2}$	311.7765	168.9821
	$^2P_{3/2}$	265.2801	122.4857	$2p^5 3p3d$	$^2F_{7/2}$	311.7851	168.9906
	$^2S_{1/2}$	266.5997	123.8057		$^2P_{1/2}$	312.8988	170.1043
	$^2D_{5/2}$	269.9206	127.1262		$^2D_{5/2}$	313.6872	170.8927
	$^2P_{3/2}$	270.6199	127.8254		$^2D_{3/2}$	313.7682	170.9737
	$^2D_{3/2}$	272.2418	129.4474		$^2P_{3/2}$	314.0546	171.2601
	$^2P_{1/2}$	272.2461	129.4517		$^2P_{1/2}$	314.0863	171.2919
	$^2S_{1/2}$	277.7961	135.0017		$^2G_{9/2}$	314.7269	171.9324
$2p^5 3p^2$	$^2P_{1/2}$	280.2715	137.4770		$^2F_{7/2}$	315.7038	172.9093
	$^2F_{7/2}$	281.1028	138.3084		$^2D_{5/2}$	316.9671	174.1726
	$^2F_{5/2}$	282.0637	139.2693		$^2S_{1/2}$	317.1615	174.3671
	$^2D_{3/2}$	282.7025	139.9091		$^2P_{3/2}$	317.3477	174.5532
	$^2D_{5/2}$	283.7537	140.9593		$^2G_{7/2}$	317.6851	174.8907
	$^2P_{3/2}$	283.9142	141.1198		$^2F_{5/2}$	318.1806	175.3862
	$^2D_{3/2}$	284.4862	141.6918		$^2D_{3/2}$	318.7976	176.0032
	$^2S_{1/2}$	285.0982	142.3037		$^2P_{1/2}$	319.2191	176.4247
	$^2D_{5/2}$	285.1238	142.3294		$^2D_{3/2}$	322.4772	179.6828
	$^2P_{3/2}$	288.6843	145.8899		$^2D_{5/2}$	322.6709	179.8769
	$^2P_{1/2}$	289.6220	146.8275	$2p^5 3d^2$	$^2F_{5/2}$	334.4696	191.6752
	$^2P_{3/2}$	291.5013	148.7068		$^2P_{1/2}$	334.6284	191.8340
$2p^5 3s3d$	$^2F_{5/2}$	292.2209	149.4264		$^2D_{5/2}$	334.7146	191.9472
$2p^5 3p^2$	$^2P_{1/2}$	289.6220	149.7103		$^2F_{7/2}$	334.8851	192.0907
$2p^5 3s3d$	$^2D_{3/2}$	292.6876	149.8932		$^2P_{3/2}$	334.9184	192.1239
	$^2F_{7/2}$	292.6939	149.8995		$^2H_{11/2}$	334.9697	192.1752
	$^2D_{5/2}$	292.9935	150.1990		$^2G_{9/2}$	335.1578	192.3634
	$^2P_{3/2}$	294.7195	151.9250		$^2F_{7/2}$	335.4651	192.6707
	$^2P_{1/2}$	294.8930	152.0986		$^2H_{9/2}$	335.9741	193.1797
	$^2F_{7/2}$	296.7125	153.9180		$^2G_{7/2}$	335.9875	193.1930
	$^2D_{5/2}$	297.4539	154.6594		$^2D_{3/2}$	336.1494	193.3550
	$^2P_{3/2}$	298.3331	155.5386		$^2D_{3/2}$	336.2396	193.4451
	$^2P_{1/2}$	298.9962	156.2017		$^2F_{5/2}$	337.0241	194.2297
	$^2F_{5/2}$	299.1797	156.3815		$^2F_{7/2}$	337.4310	194.6366
	$^2D_{3/2}$	300.5103	157.7078		$^2D_{5/2}$	337.6095	194.8151
$2p^5 3s3d$	$^2F_{5/2}$	305.2175	162.4230		$^2S_{1/2}$	337.9793	195.1849
	$^2D_{3/2}$	305.4196	162.6252		$^2F_{5/2}$	337.9801	195.1857
	$^2F_{7/2}$	305.6947	162.9002		$^2G_{9/2}$	338.0955	195.3011
	$^2G_{7/2}$	306.0547	163.2602		$^2G_{7/2}$	339.1949	196.4005
	$^2P_{1/2}$	306.2334	163.4389		$^2D_{5/2}$	339.9540	196.7297
	$^2G_{9/2}$	306.2387	163.4442		$^2D_{3/2}$	339.6574	196.8630
	$^2D_{5/2}$	307.3780	164.5836		$^2P_{1/2}$	339.7694	196.8849
	$^2P_{3/2}$	307.7796	164.9851		$^2P_{3/2}$	340.3524	197.5580
	$^2F_{7/2}$	307.8657	165.0712		$^2P_{3/2}$	342.2280	199.4335
	$^2F_{5/2}$	307.9886	165.1941		$^2P_{1/2}$	344.1505	201.3560
	$^2F_{5/2}$	309.5919	166.7975				

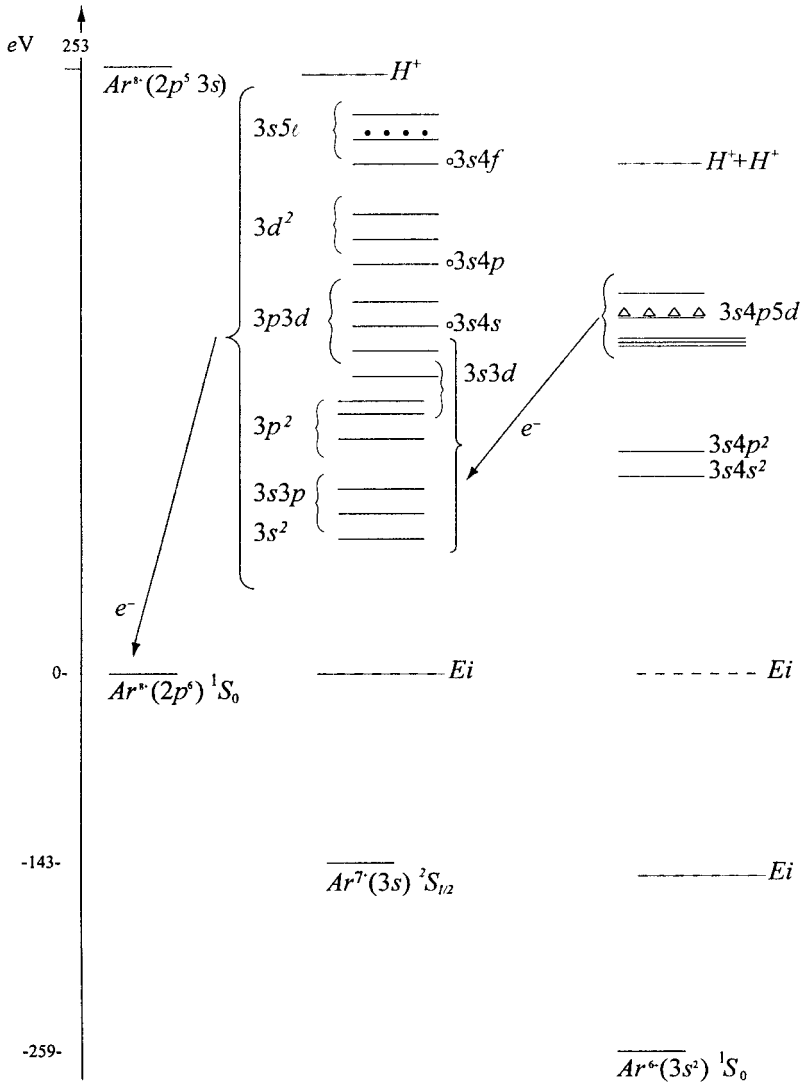

FIG. 6. Overall level diagram showing column 1 (left), the entrance channel $Ar^{8+}(2p^5 3s)\,^3P_{0,2}$; column 2 (center), the SC exit channel (upper part) and the levels $2p^5 3l3l'$ populated by the first Auger transition following DC; column 3 (right), DC exit channels. Center of the reaction window: △, DC; ●, SC.

$$\omega_T = \Sigma A_r^{ii}/(\Sigma A_r^{ii} + \Sigma A_a^{si}), \tag{7}$$

$$B_r = A_a^{si}/(\Sigma A_r^{ii} + \Sigma A_n^{si}), \tag{8}$$

where A_r^{ij} and A_a^{si} are the transition probabilities and the Auger rates, respectively.

To perform the calculation of the atomic data, we have chosen the following configurations: $1s^2 2s^2 2p^6 3s$ for the ground state, $2p^6 nl$ and $2p^5 3snl$ for the singly and doubly excited states of the Na-like Ar ion, respectively, with $n=5$ and $l=0 \rightarrow n-l$; the n and l values are determined by using different experimental scaling rules [7–10]. This choice leads to 11 configurations, 45 terms in *LS* coupling, and 106 levels in *LSJ* coupling. The calculated data are presented for $2p^5 3s5l$ with $l=0$, 1, 2, 3, and 4 in Table I. This set of results extends previously published data that were given up to $4l$ [3]. In Table II we give the energies of $Ar^{7+}(2p^5 3l3l')$ since these levels appear to be the intermediate continua in the decay following DC [1]. For DC by the metastable ion, we end up in the formation of triply excited ions. An accurate calculation of the Mg-like triply excited levels with any code is very difficult. Moreover, given the limited reliability of the code we used previously [1], we proceed along two directions.

(i) First, we use the predictive procedure to estimate the collision translational energy gain window (in the energy scale) where DC most likely ends up. Clearly, we assume that the projectile energy gains are the same as in DC by the ground-state projectile Ar^{8+} in $Ar^{8+}+H_2$; we have observed an energy gain [12] peaking at 50 eV and centered on the $(4l5l')$ levels. Since core conservation of the metastable ion is expected, DC populate mostly $Ar^{6+}(2p^5 3s4l5l')$; their positions are shown in Fig. 6 (the center of the collision window is shown in the form of open triangles).

(ii) Second, a trial was performed to estimate theoretically the energetic positions of these levels with respect to the ground state of the Mg-like ion. Some of the results are obtained using the SUPERSTRUCTURE code; the values are given in Table III, they overlap satisfactorily with the results deduced from our assumptions on the energy gains (see above and Fig. 6).

It is now possible to identify the major transitions in both spectra (Fig. 3, X-VUV spectrum and Fig. 5, Auger spec-

TABLE III. Energy levels for $Ar^{6+}(2p^5 3s4l5l')$ relative to the ground state. Column 1: level designation; column 2: energy (eV) from ground state Ar^{6+}; column 3: energy (eV) from ground state Ar^{8+}.

Level designation		Energy (eV) per GS	Energy (eV) per Ar^{8+}
$2p^5 3s4s5s$	$^5P_3$	411.4289	146.9638
	$^5P_2$	411.6269	147.1618
	$^3P_1$	412.0917	147.6266
	$^3P_2$	412.5180	148.0529
	$^3P_0$	412.5319	148.0668
	$^3P_1$	413.0818	148.6167
	$^5P_1$	413.7202	149.2551
	$^3P_2$	413.7206	149.2555
	$^1P_2$	414.0817	149.6166
$2p^5 3s4s5p$	$^5S_2$	414.3550	149.8899
	$^5D_4$	414.4912	150.0261
	$^5D_3$	414.5665	150.1014
$2p^5 3s4s5d$	$^3P_2$	414.5737	150.1086
	$^3P_0$	414.6641	150.1990
$2p^5 3s4s5p$	$^3D_3$	414.7415	150.2764
	$^3P_2$	414.7485	150.2834
	$^3S_1$	414.9109	150.4458
	$^5P_1$	415.0687	150.6033
	$^3S_1$	418.1396	153.6745
$2p^5 3s4p5s$	$^5S_2$	418.1396	153.6745
$2p^5 3s4s5d$	$^1P_1$	421.2103	156.7452
$2p^5 3s4p5p$	$^5P_1$	421.2509	156.7858
	$^3P_2$	421.3393	156.8742
	$^5P_2$	421.3516	156.8865
	$^3P_2$	425.2740	160.8089
$2p^5 3s4p5d$	$^5D_0$	425.2817	160.8166
	$^5D_1$	425.2903	160.8252
	$^5D_2$	425.3028	160.8377
	$^5D_3$	425.3147	160.8496
$2p^5 3s4p5p$	$^3P_1$	425.3233	160.8582
$2p^5 3s4p5d$	$^3D_3$	427.8195	163.3544
$2p^5 3s4d5s$	$^5P_1$	427.8364	163.3713
	$^3D_2$	430.7432	166.2781
$2p^5 3s4d5p$	$^5D_1$	430.7802	166.3151
	$^5D_1$	434.3542	169.8891
$2p^5 3s4d5d$	$^3H_4$	435.4480	170.9829
	$^1P_1$	441.1032	176.6381

trum). Clearly, it is not possible to deduce absolute intensity values: the physical reason is that there is no method available to cross calibrate an X-VUV spectrometer against an Auger spectrometer.

IV. IDENTIFICATIONS AND COLLISION FEATURES

It is possible to describe the capture processes by the metastable projectile colliding with H_2 in the following way. For SC

$$Af^{8+}(2p^5 3s)^3P_{0,2}+H_2 \rightarrow Ar^{7+}{**}(2p^5 3s\, nl)^{2,4}L_J+H_2^+ \tag{9}$$

with $n=5$ mostly and 4. This is followed by

$$Ar^{7+}{**} \rightarrow Ar^{8+}(2p^6)^1S_0+e^-(\text{Auger decay}) \tag{10}$$

and/or cascade ending in

$$Ar^{7+}{**} \rightarrow Ar^{7+}(3s)^2S_{1/2}+h\nu. \tag{11}$$

For DC

$$Ar^{8+}(2p^5 3s)^3P_{0,2}+H_2 \rightarrow Ar^{6+}{***}(2p^5 3s\, nl\, n'l')+H^+ +H^+ \tag{12}$$

followed by two autoionization steps

$$Ar^{6+}{***}(2p^5 3s\, nl\, n'l') \rightarrow Ar^{7+}{**}(2p^5 3l3l')+e^-(\text{low energy}). \tag{13}$$

This first step is followed by:

$$Ar^{7+}{**}(2p^5 3l3l') \rightarrow Ar^{8+}(2p^6)^1S_0+e^-(\text{high energy}). \tag{14}$$

There is a nonzero probability for some radiative decay after DC: given the limited resolution and the low metastable fraction in the incident ion beam, we do not expect to be able to separate any of these rays. Physically these are hypersatellites to the parent transitions shown in Fig. 4.

A. X-VUV spectroscopy

The spectrum in the wavelength range 40–54 Å (Fig. 3) demonstrates the complexity of the line identification. Unambiguously, the spectrum corresponds to the decay process following capture by the metastable projectile. The most intense transitions, identified by using the theoretical data, are underlined in Table IV. For example, the most intense transition is $1s^2 2s^2 2p^5 3s\,4d\,^4D_{1/2} \rightarrow 1s^2 2s^2 2p^6 5s\,^2S_{1/2}$ at 51.51 Å. A remarkable feature is that most of these transitions correspond to the following process: two electrons change their orbitals and one photon is emitted [15]. The upper quartet states are more populated than the doublets. This reflects the statistical J-sharing and confirms previous observations in charge-transfer collisions [16], where for a given L the highest J value is mostly populated. Moreover, given the importance of the transitions from upper levels with outer orbital $4l$, we would emphasize the possibility of {SC+dissociation}, as observed in the case of the ground-state projectile colliding with H_2 [12]. Some cascade feeds from $5l$ states to $4l'$ are possible, given the large values of their fluorescence yields. This appears in the underlined values of ω_T close to l in Table I. This is supported by the fact that in highly excited systems (n large), the direct decay to the lowest-lying level has a low branching ratio value favoring cascades to intermediate levels ([12] and references therein). This argument would explain the intensity of the transitions from $4l$.

TABLE IV. Tentative XUV line assignments. The major line assignments are underlined in the table. Column 1: transitions; column 2: calculated wavelengths (Ångstroms); column 3: transition probabilities; column 4: experimental wavelengths; column 5: intensities (arbitrary units).

Transitions	λ_{th} (Å)	A_r (s^{-1})	λ_{ext} (Å)	Intensity counts
$1s^22s^22p^53s4d\ ^2P_{1/2}-1s^22s^22p^65s\ ^2S_{1/2}$	50.9231	1.521+08	50.92	208.2
$1s^22s^22p^53s4d\ ^2P_{3/2}-1s^22s^22p^65s\ ^2S_{1/2}$	50.9355	1.945+08	50.98	204.5
$1s^22s^22p^53s4d\ ^2D_{3/2}-1s^22s^22p^65s\ ^2S_{1/2}$	51.0696	1.272+06	51.06	217.8
$1s^22s^22p^53s4d\ ^2D_{3/2}-1s^22s^22p^65s\ ^2S_{1/2}$	51.2255	1.014+08	51.22	233.1
$1s^22s^22p^53s4d\ ^4D_{3/2}-1s^22s^22p^65s\ ^2S_{1/2}$	51.4299	9.149+07	51.42	250.0
$1s^22s^22p^53s4d\ ^4D_{1/2}-1s^22s^22p^65s\ ^2S_{1/2}$	51.5199	1.798+08	51.51	237.7
$1s^22s^22p^53s4d\ ^2P_{3/2}-1s^22s^22p^65s\ ^2S_{1/2}$	51.5540	3.837+07	51.55	216.7
$1s^22s^22p^53s4d\ ^2P_{1/2}-1s^22s^22p^65s\ ^2S_{1/2}$	51.5724	8.858+07	51.58	204.8
$1s^22s^22p^53s4d\ ^4F_{3/2}-1s^22s^22p^65s\ ^2S_{1/2}$	51.6475	2.031+07	51.64	202.1
$1s^22s^22p^53s4d\ ^4P_{3/2}-1s^22s^22p^65s\ ^2S_{1/2}$	51.8297	8.387+05	51.83	145.6
$1s^22s^22p^53s4d\ ^4P_{1/2}-1s^22s^22p^65s\ ^2S_{1/2}$	51.8602	1.865+05	51.86	151.3
$1s^22s^22p^53s4d\ ^2P_{1/2}-1s^22s^22p^65d\ ^2D_{3/2}$	52.4718	1.262+08	52.47	87.43
$1s^22s^22p^53s4d\ ^2P_{3/2}-1s^22s^22p^65d\ ^2D_{5/2}$	52.4872	1.415+08	52.49	84.77
$1s^22s^22p^53s4d\ ^2P_{3/2}-1s^22s^22p^65d\ ^2D_{3/2}$	52.4849	1.061+07	52.49	84.77
$1s^22s^22p^53s4d\ ^2D_{5/2}-1s^22s^22p^65d\ ^2D_{3/2}$	52.5926	1.808+06	52.58	79.12
$1s^22s^22p^53s4d\ ^2D_{5/2}-1s^22s^22p^65d\ ^2D_{5/2}$	52.5949	3.362+05	52.58	79.12
$1s^22s^22p^53s4d\ ^2D_{3/2}-1s^22s^22p^65d\ ^2D_{5/2}$	52.6274	9.281+05	52.63	79.12
$1s^22s^22p^53s4d\ ^2D_{3/2}-1s^22s^22p^65d\ ^2D_{3/2}$	52.6997	2.181+05	52.63	79.12
$1s^22s^22p^53s4d\ ^2F_{7/2}-1s^22s^22p^65d\ ^2D_{5/2}$	52.6641	2.933+05	52.65	79.45
$1s^22s^22p^53s4d\ ^2F_{5/2}-1s^22s^22p^65d\ ^2D_{3/2}$	52.6665	3.697+05	52.65	79.45
$1s^22s^22p^53s4d\ ^2D_{3/2}-1s^22s^22p^65d\ ^2D_{3/2}$	52.6743	1.775+06	52.67	80.11
$1s^22s^22p^53s4d\ ^2D_{3/2}-1s^22s^22p^65d\ ^2D_{3/2}$	52.7943	7.147+06	52.79	74.45
$1s^22s^22p^53s4d\ ^4D_{5/2}-1s^22s^22p^65d\ ^2D_{3/2}$	52.8504	1.050+05	52.85	79.1
$1s^22s^22p^53s4d\ ^2S_{1/2}-1s^22s^22p^65d\ ^2P_{1/2}$	53.2142	6.077+08	53.21	81.73
$1s^22s^22p^53s4d\ ^2S_{1/2}-1s^22s^22p^65p\ ^2P_{3/2}$	53.2279	1.947+08	53.23	83.38

B. Auger-electron spectroscopy

The identification procedure obliges us to consider the high- and the low-energy ranges separately. In the range extending from 100 eV up to 250 eV (see Fig. 5)—of weaker intensity than the low-energy part—one distinguishes two parts shown as recorded and magnified by a factor of 5: the part above 200 eV which unambiguously is due to the Auger decay into the only available continuum $Ar^{8+}(2p^6)^1S_0$, following SC to the metastable core. Even though the identification of the Auger lines is complex, we propose the tentative assignments as shown in Table V. The levels $1s^22s^22p^53s5s$ and $5p$ in the suggested assignments are characterized by extremely small fluorescence yields as appears in Table I. The uncertainties of the experimental values

TABLE V. Tentative Auger line assignments for the stabilization following SC by the metastable projectile. Column 1: experimental energy values of Auger transitions from $n=5$; column 2: amplitude (arbitrary units); column 3: level assignments; column 4: calculated energies.

Experimental energies (eV)	Amplitudes (a.u.)	Assignments	Calculated energies (eV)
$209.1 \leqslant E \leqslant 210.2$	$0.95 \leqslant A \leqslant 1.1$	$1s^22s^22p^53s5s\ ^4P_{5/2}$	210.85
$210.3 \leqslant E \leqslant 212.1$	$0.75 \leqslant A \leqslant 0.93$	$1s^22s^22p^53s5s\ ^4P_{3/2}$	211.26
$210.3 \leqslant E \leqslant 212.1$	$0.75 \leqslant A \leqslant 0.93$	$1s^22s^22p^53s5s\ ^2P_{3/2}$	212.03
213.50	0.81	$1s^22s^22p^53s5s\ ^4P_{1/2}$	213.12
214.10	0.98	$1s^22s^22p^53s5s\ ^2P_{1/2}$	214.65
215.00	0.70	$1s^22s^22p^53s5s\ ^4P_{1/2}$	214.95
215.50	0.54	$1s^22s^22p^53s5s\ ^2S_{1/2}$	215.50
216.30	0.75	$1s^22s^22p^53s5s\ ^4D_{1/2}$	216.39

are of the order 0.15 eV. The assigned upper levels confirm that the capture process is core conserving and has populated $3s5s$ and $3s5p$. The part from 100 eV up to nearly 200 eV has to be considered together with the low-energy part which is seen from 0 to 60 eV (Fig. 5).

We consider the range 100 eV to less than 200 eV. To ease the identifications, we have recalculated all the level energies of $Ar^{7+}(2p^5 3l\,3l')$ relative to the ground state and these are given in Table II with the energy of the Auger electrons. The corresponding range is indicated in Fig. 5 in the high-energy part of the spectrum. These lines are attributed to the second Auger step following DC. Since the SC reaction window is centered on $n=5$, and as the process is assumed to be core conserving, we can conclude that the population mechanisms of these states result from a first Auger transition to these states for which they are the intermediate continua. For example, the peaks at ~136 and 183 eV are attributed to the decay of $2p^5 3p^2$ and $2p^5 3d^2$, respectively. These last levels are the continua to which some of the $Ar^{6+***}(2p^5 3s\,nl\,n'l')$ states decay with the emission of a low-energy electron.

The identification of the rays associated with this first step is very difficult: they are of weak amplitude (the metastable fraction content in the incident beam is no more than 5–6 %) and they are merged among high amplitude transitions due to the stabilization following the DC by the ground-state ion [12]. Moreover, given the number of populated levels and the extent of the energy overlap between the Na-like core excited levels (the continua for the first Auger step) and the Mg-like core excited levels (see Fig. 6), the number of possible transitions is numerically important. The corresponding energies are probably distributed in the range from 10 to 50 eV (in Fig. 6, the arrow from column 3 to column 2 gives the extent of the energy spread of these transitions). For example, given the energy of the group of levels $Ar^{6+}(2p^5 3s\,4d\,5p)^5 D_1^e$ in the energy range 430.78 to 434.35 eV from the ground state, a possible first Auger decay to $Ar^{7+}(2p^5 3p\,3d)L_J$ would give electrons with energies between 11.5 and 20.8 eV.

One major issue is that the selection rules for these transitions are still an open question. Another difficult problem that has not been addressed so far is the calculation of Auger probabilities, when, for a given upper level, more than one continuum is available to which the transition may occur. In the present case, this adds to the difficulty of line identification. This raises as well the question of calculating the lifetimes for these transitions of very low energies.

V. CONCLUSION

We have shown that the characteristics of SC and DC are the same for Ar^{8+} ions in the ground and in the metastable $^3P_{0,2}$ states. For metastable Ar^{8+} ions colliding with H_2, SC dominantly populates states with $n=5$. The calculated atomic data have been used to identify the stabilization of these states, sharing among radiation and Auger decays.

The DC stabilization takes place via a two-step Auger process. The first step in the Auger decay gives transitions from core-conserved states, which are overlapping with the spectrum of DC by the ground-state ion (energies in the range 0–60 eV). The transitions of the second Auger series are associated with cores differing from the initial ones, as they are formed by the first Auger process. A direct population of these states by capture can be excluded due to the core-conserving character of this process.

The dissociation of the H_2 molecule during the capture collision probably takes place with the metastable projectile as with the ground projectile. The importance of the optical transitions seen with upper states in $n=4$ could be related to this process [12]. However, to a certain extent these $n=4$ levels are also populated by cascades.

This experimental approach makes possible the observation of transitions otherwise named dielectronic recombination satellites, as usually observed in hot plasmas. In this experimental approach, they are separated from the parent transitions (Figs. 3 and 4).

The Auger cascade decay of triply excited ions via two steps is of interest since this can be an approach to start the analysis of experimental situations met in the observation of multiply charged ion/surface interactions, where multiply excited ions are formed.

The identification procedure was based on the use of the scaling rules. Their validity is confirmed. This conclusion is important since in this type of experimental situation no theoretical collision description exists.

A question is open for further developments: when a multiply excited ion shares its stabilization between radiation and autoionization, is there the possibility to cross calibrate an X-VUV spectrometer against an Auger spectrometer in order to determine absolute fluorescence yields?

[1] S. Bliman, M. Cornille, B. A. Huber, and J. F. Wyart, Phys. Rev. A **56**, 4683 (1997).

[2] S. Bliman, M. G. Suraud, D. Hitz, B. A. Huber, H. Lebius, M. Cornille, J. E. Rubensson, J. Nordgren, and E. J. Knystautas, Phys. Rev. A **46**, 1321 (1992).

[3] S. Jacquemot, M. Cornille, and J. Nielsen, Phys. Scr. **58**, 203 (1998).

[4] J. Nordgren and R. Nyholm, Nucl. Instrum. Methods Phys. Res. B **9**, 314 (1985).

[5] E. M. Mack, Ph.D. thesis, University of Utrecht, The Netherlands, 1987 (unpublished).

[6] M. Boudjema, Ph.D. thesis, University of Algiers, Algeria, 1990 (unpublished).

[7] H. Ryufuku, K. Sasaki, and T. Watanabe, Phys. Rev. A **21**, 745 (1980).

[8] R. Mann, F. Folkmann, and H. F. Beyer, J. Phys. B **14**, 1161 (1981).

[9] A. Barany *et al.*, Nucl. Instrum. Methods Phys. Res. B **9**, 397 (1985).

[10] A. Niehaus, J. Phys. B **19**, 2925 (1986).

[11] R. Hutton, D. Schneider, and M. H. Prior, Phys. Rev. A **44**, 243 (1991).
[12] S. Bliman, M. Cornille, B. A. Huber, H. Lebius, A. Langereis, J. Nordgren, and R. Bruch, Phys. Rev. A **60**, 2799 (1999).
[13] W. Eissner and H. Nussbaumer, Comput. Phys. Commun. **8**, 270 (1974).
[14] J. Dubau and M. Loulergue (TFR Group), J. Phys. B **15**, 1907 (1981).
[15] S. Bliman, P. Indelicato, D. Hitz, P. Marseille, and J. P. Desclaux, J. Phys. B **22**, 2741 (1989).
[16] S. Bliman, R. Bruch, P. L. Altick, D. Schneider, and M. H. Prior, Phys. Rev. A **53**, 4176 (1996).